CrossMark

ORIGINAL PAPER

Progressive accumulation of autofluorescent granules in macrophages in rat striatum after systemic 3-nitropropionic acid: a correlative light- and electron-microscopic study

Tae-Ryong Riew[1] · Hong Lim Kim[2] · Jeong-Heon Choi[1] · Xuyan Jin[1] · Yoo-Jin Shin[1] · Mun-Yong Lee[1]

Abstract A variety of tissue biomolecules and intracellular structures are known to be autofluorescent. However, autofluorescent signals in brain tissues often confound analysis of the fluorescent markers used for immunohistochemistry. While investigating tissue and cellular pathologies induced by 3-nitropropionic acid, a mitochondrial toxin selective for striatal neurons, we encountered many autofluorescent signals confined to the lesion core. These structures were excited by blue (wavelength = 488 nm) and yellow-orange (555 nm), but not by red (639 nm) or violet (405 nm) lasers, indicating that this autofluorescence overlaps with the emission spectra of commonly used fluorophores. Almost all of the autofluorescence was localized in activated microglia/macrophages, while reactive astrocytes emitted no detectable autofluorescence. Amoeboid brain macrophages filled with autofluorescent granules revealed very weak expression of the microglial marker, ionized calcium-binding adaptor molecule 1 (Iba1), while activated microglia with evident processes and intense Iba1 immunoreactivity contained scant autofluorescent granules. In addition, immunolabeling with two lysosomal markers, ED1/CD68 and lysosomal-associated membrane protein 1, showed a pattern complementary with autofluorescent signals in activated microglia/macrophages, implying that the autofluorescent structures reside within cytoplasm free of intact lysosomes. A correlative light- and electron-microscopic approach finally revealed the ultrastructural identity of the fluorescent granules, most of which matched to clusters of lipofuscin-like inclusions with varying morphology. Thus, autofluorescence in the damaged brain may reflect the presence of lipofuscin-laden brain macrophages, which should be taken into account when verifying any fluorescent signals that are likely to be correlated with activated microglia/macrophages after brain insults.

Keywords Autofluorescence · Lipofuscin · 3-NP · Microglia · Macrophages · Lysosome

Introduction

It is well known that stimulation with the appropriate wavelengths of light can cause biological tissues to exhibit a fluorescence emission, autofluorescence, in the absence of exogenous fluorophores (Aubin 1979; Croce et al. 1999; Monici 2005), and that these nonspecific signals can interfere with the fluorescence signal of interest to produce false-positive results. Tissue autofluorescence can be caused by formaldehyde fixation and by biomolecules such as lipofuscin, flavin, porphyrin, nicotinic coenzymes, collagen, elastin, and the neurotransmitter serotonin (Aubin 1979; Banerjee et al. 1999; Crespi et al. 2004; Viegas et al. 2007; Ottis et al. 2012). We focus here on lipofuscin, a complex mixture of oxidized protein and lipid degradation residues that accumulates progressively over time in the lysosomes of post mitotic cells such as cardiomyocytes and neurons (Terman and Brunk 1998; Boellaard et al. 2004; Gray and Woulfe 2005; Jung et al. 2007). The amount and spatial distribution of these endogenous fluorophores may be affected by pathological or experimental conditions,

✉ Mun-Yong Lee
munylee@catholic.ac.kr

1   Department of Anatomy, Catholic Neuroscience Institute, Cell Death Disease Research Center, College of Medicine, The Catholic University of Korea, 222 Banpo-daero, Seocho-gu, Seoul 06501, Republic of Korea

2   Integrative Research Support Center, Laboratory of Electron Microscope, College of Medicine, The Catholic University of Korea, Seoul, Republic of Korea

resulting in changes in autofluorescence emission. Several studies have shown that autofluorescence increased in damaged brain tissue (Brooke et al. 1996; Chung et al. 1997; Liu et al. 2002; Spanswick et al. 2009) and is associated with aging (Brizzee et al. 1974; Amenta et al. 1988).

While examining the pathological features of rats treated with 3-nitropropionic acid (3-NP), a natural mitochondrial toxin that selectively impairs medium-spiny striatal neurons (Hamilton and Gould 1987), we encountered strong autofluorescence in the lesion core region abutting the astroglial scar over the 2-week, post-injury time period. This autofluorescence emission appeared to develop concomitantly with neurodegeneration, and had a spectrum overlapping with the emissions of commonly used fluorescent dyes. Since this nonspecific fluorescence could blur the distinction between specific and nonspecific fluorescence signals, and thus interfere with the interpretation of fluorescence labeling, we saw a strong need to define exactly the characteristics of the autofluorescence occurring within sites of intense neural damage after brain insults. We offer a solution to the interference problem based on our spectral experiments, as well as offering ultrastructural elucidation capable of informing other solutions should the spectral solution be unsuitable in some context.

The purpose of the present study is to define the spectral and structural details of the autofluorescent signals induced by 3-NP injection. Given the limitations of light microscopy for precise localization of autofluorescence to specific organelles and subcellular structures, we applied a method that allows the researcher to correlate the light microscopic signals with the respective subcellular structures as visualized by electron microscopy. This correlative approach offers an informative and efficient way to identify specific targets for further examination at the ultrastructural level. The present investigation provides the first direct identification of autofluorescent granules within the striatal 3-NP lesion core as clusters of lipofuscin-like granules within brain macrophages.

Materials and methods

Animal preparation

All experimental procedures were conducted in accordance with the Laboratory Animal Welfare Act, the Guide for the Care and Use of Laboratory Animals, and Guidelines and Policies for Rodent Survival Surgery, and were approved by the Institutional Animal Care and Use Committee at the College of Medicine, The Catholic University of Korea (Approval Number: CUMC-2016-0014-02). All efforts were made to minimize animal suffering and to reduce the number of animals used.

Adult, male Sprague–Dawley rats (250–300 g, aged 9–11 weeks) were used in this study. Animals were housed in groups of three per cage in a controlled environment at a constant temperature (22 ± 5 °C) and humidity (50 ± 10%) with food (gamma ray-sterilized diet) and water (autoclaved tap water) available ad libitum. They were maintained on a 12-h light/dark cycle. 3-NP (Sigma-Aldrich, St. Louis, MO, USA) was dissolved in buffered saline (pH = 7.0), and administered intraperitoneally (i.p.) at a dose of 15 mg/kg once daily for 3 days. All 3-NP-injected rats were evaluated daily for the presence of behavioral deficit, and only rats exhibiting neurological deficit symptoms, including hind limb impairment or kyphotic posture, recumbency, and impaired postural adjustments, were included in the experimental group (Hamilton and Gould 1987).

Animals were killed at 3, 7, 14, and 28 days after the final injection of 3-NP ($n = 3$ rats for each time point). The control group ($n = 3$) received intraperitoneal injections of the same volume of normal saline for three consecutive days and were killed 3 days after the final injection. The animals were perfused transcardially with 4% paraformaldehyde in 0.1 M phosphate buffer (PB; pH = 7.4) after being anesthetized with 10% chloral hydrate (4 mL/kg i.p.). The brain tissues were equilibrated with 30% sucrose in 0.1 M PB and fully frozen.

Immunohistochemistry and Sudan Black B staining

To visualize autofluorescent materials in the 3-NP–injected rat brain, coronal cryostat sections 25 µm thick were labeled with 4′,6-diamidino-2′-phenylindole (DAPI, Roche Mannheim, Germany; 1:2000) for 10 min. Sections were then coverslipped with Fluoroshield (ImmunoBioScience, Mukilteo, WA, USA). A separate series of serial cryostat sections was incubated overnight at 4 °C with one of the following antibodies: mouse monoclonal antibody to glial fibrillary acidic protein (GFAP; 1:1500; Millipore, Temecula, CA, USA), ED1 (CD68; 1:100; Bio-Rad, Hercules, CA, USA), rabbit polyclonal antibodies to ionized calcium-binding adaptor molecule 1 (Iba1; 1:500; Wako Pure Chemical Industries, Ltd., Osaka, Japan), or lysosomal-associated membrane protein 1 (LAMP1; 1:200; Abcam, Cambridge, UK). Antibody staining was visualized with Alexa Fluor 647-tagged goat anti-rabbit antibodies or with goat anti-mouse antibodies (1:300; Molecular Probes, Inc., Eugene, OR, USA). The specificity of immunoreactivity was confirmed by the absence of immunohistochemical staining in sections from which the primary or secondary antibody had been omitted. Control sections were prepared as described above. Counterstaining of cell nuclei was carried out in DAPI solution for 10 min. Slides were viewed with a confocal microscope (LSM 700; Carl Zeiss Co. Ltd.,

Oberkochen, Germany) equipped with four lasers (Diode 405, Argon 488, HeNe 555, and HeNe 639).

To confirm the autofluorescent cell contents as lipofuscin-like, a 0.1% solution of Sudan Black B (Sigma-Aldrich) in 70% ethanol was prepared. Coronal cryostat sections were immersed in 0.1% Sudan Black B solution for 5 min at room temperature. The sections were washed three times with distilled water, and nuclei were counterstained with 0.1% Nuclear Fast Red (Vector, Burlingame, CA, USA). Tissue sections were visualized using a microscope and photographed using a digital camera (Jenoptik, Germany). To visualize autofluorescence, serial sections were labeled with DAPI and viewed with a confocal microscope as described above. All images were converted to TIFF format. Contrast levels and image sizes were adjusted using Adobe Photoshop v.10.0.

Quantification and statistics

Intensity profiles of specific areas were obtained using Zen 2010 (Carl Zeiss Co. Ltd.). Scatterplot and correlation analysis was performed with Excel 2013 (Microsoft, Bellevue, WA, USA).

To quantify the time-dependent changes in ED1/CD68-positive cells containing autofluorescence in striatum subjected to 3-NP, confocal microscopic images of ED1/CD68-immunolabeled tissue sections from experimental rats at 3, 7, 14, and 28 days post-injection ($n = 3$ per time point) were obtained from the invariable region between levels 0.24 mm and 1.56 mm dorsal (Paxinos and Watson 1998). Five areas of 160×160 µm per field were selected in the lesion core of each section and captured at $400\times$ magnification under constant viewing conditions. ED1/CD68-positive cells with or without autofluorescence were counted, but only when their nuclei could be seen clearly. The data are presented as the mean ± SEM, and the differences in cell counts between different time points were assessed with two-tailed, unpaired Student's t tests using Excel 2013 (Microsoft, Bellevue, WA, USA) and GraphPad Prism, Version 5 (GraphPad Software Inc., San Diego, CA, USA). Differences with P values of less than 0.05 were considered statistically significant.

Ultrastructural analysis and correlative light and electron microscopy

The electron microscopic (EM) study used rats at 28 days of survival after the last injection of 3-NP ($n = 3$). Serial vibratome sections 50 µm thick were prepared. For conventional EM, sections were post-fixed with 2.5% glutaraldehyde and 1% osmium tetroxide in 0.1 M PB for 30 min. Other serial sections were used for pre-embedding, immunoperoxidase EM. Sections were incubated with a rabbit polyclonal antibody to Iba1 (1:500) overnight at 4 °C. Primary antibody binding was visualized using peroxidase-labeled goat anti-rabbit IgG (1:100; Jackson ImmunoResearch, West Grove, PA, USA), and 0.05% 3,3′-diaminobenzidine tetrahydrochloride (DAB), with 0.01% H_2O_2 as the substrate. After post-fixation with 2.5% glutaraldehyde and 1% osmium tetroxide in 0.1 M PB for 30 min, the tissues were dehydrated in graded alcohols and embedded in Epon 812 resin. The areas of interest were then excised and glued onto resin blocks. After cutting into ultrathin sections of 70–90 nm thickness and staining with 1% uranyl acetate, they were placed on copper grids and observed in a transmission electron microscope (TEM; JEM 1010, JEOL, Tokyo, Japan).

For correlative EM, vibratome sections 100 µm thick were cryoprotected with 2.3 M sucrose in 0.1 M PB and frozen in liquid nitrogen. Semithin cryosections 2 µm thick were then cut at −100 °C with a glass knife in a Leica EM UC7 ultramicrotome equipped with the FC7 cryochamber (Leica, Wetzlar, Germany). The sections were incubated at 4 °C overnight with a rabbit polyclonal antibody to Iba1 (1:500), followed by Alexa Fluor 647-tagged goat anti-rabbit antibody (1:300). The sections were then labeled with DAPI for 10 min. Coverslipped sections were examined with a confocal microscope and photographed at various magnifications with a differential interference contrast (DIC) setting to find specific areas for later examination by EM. After the coverslips had been floated off the sections, the tissues were prepared further for EM, as described above. To localize the autofluorescence signals observed by light microscopy, distinctive morphological profiles of cell nuclei or vascular profiles within areas of interest, previously visualized with DIC microscopy, were matched with their counterparts in the ultrathin sections.

Results

Using DAPI-labeled sections, we first examined autofluorescent emissions from the striatal lesion during the experimental period following 3-NP injection. Autofluorescence was absent or negligible in the striatum of saline-treated control rats (Fig. 1a), but became evident in rats at 3 days (Fig. 1b) and 7 days (Fig. 1c) post-lesion. On day 14 post-lesion (Fig. 1d, e), reproducible, prominent autofluorescence could be detected in 3-NP-induced striatal lesions, this being more prominent at 28 days (Fig. 1f–k). As shown in Fig. 1h–l, autofluorescence was prominent with both the blue laser (excitation/emission wavelengths, 488 nm/523 nm) and the yellow-green laser (555 nm/573 nm). However, no detectable autofluorescence was observed using violet (405 nm/460 nm) or red lasers (639 nm/660 nm). The autofluorescence appeared
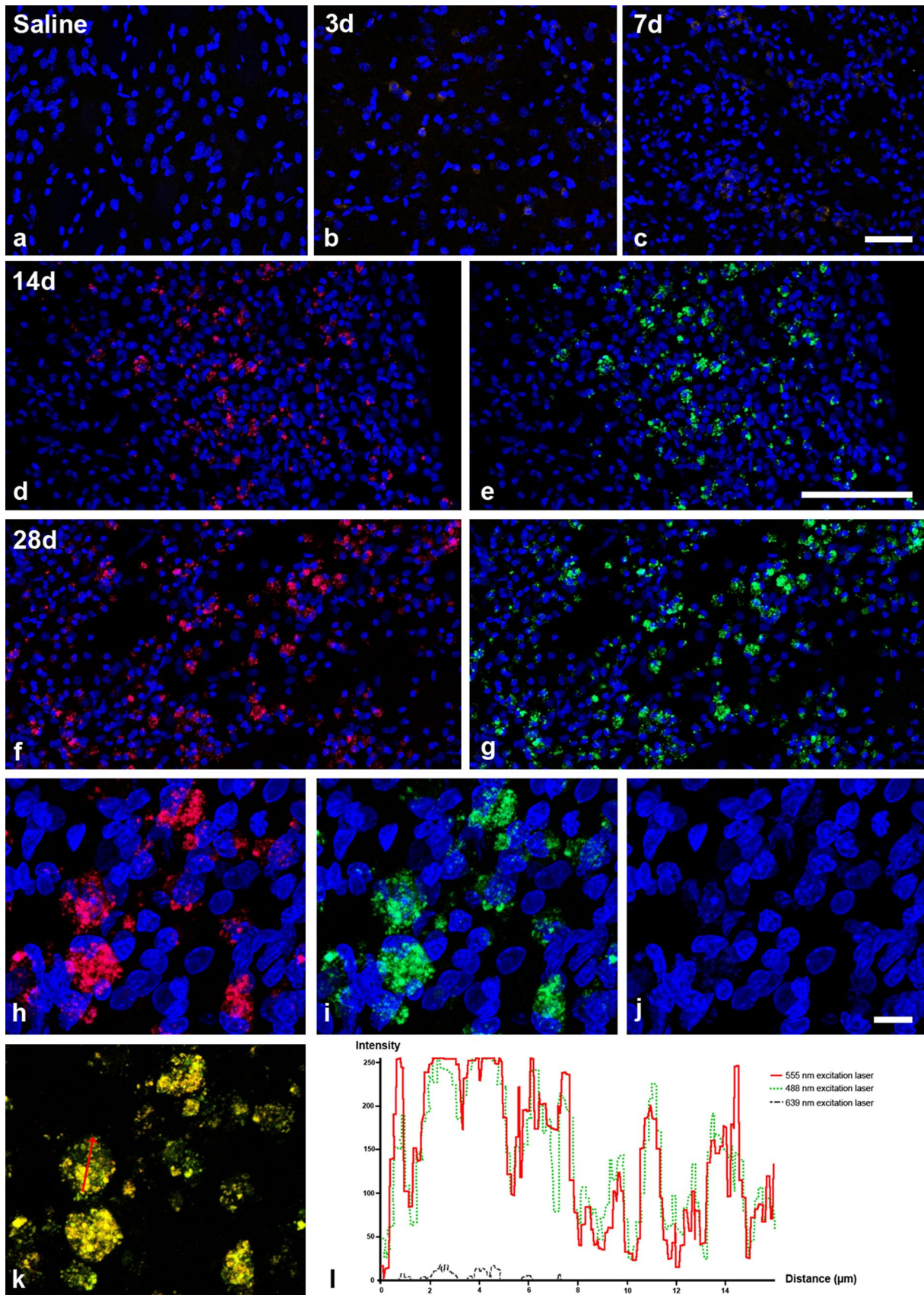
◄**Fig. 1** Temporal pattern and excitation spectral response of auto-fluorescent granules found in the lesion core of the 3-NP–treated rat brain. Representative striatal sections of saline-treated control (**a**), and experimental rats at 3 (**b**) and 7 (**c**) days post-lesion. No significant fluorescent signals can be observed with excitation by the yellow-green (555 nm) or blue laser (488 nm) in any section of control striatum, while weak but evident autofluorescence is detected by 3 days post-lesion. Cell nuclei are visualized with DAPI. Accumulations of prominent autofluorescent signals detected with yellow-green (**d**, **f**) and blue laser (**e**, **g**) in the striatal lesion core of 3-NP–treated rats at 14 days (**d**, **e**) and 28 days (**f**, **g**) post-lesion. Note that clusters of autofluorescent granules tend to increase in number and intensity by 28 days compared with 14 days. Excitation by violet laser (405 nm) is used to detect nuclear staining with DAPI. Higher-magnification views of autofluorescent granules excited with yellow-green (**h**), blue (**i**), red (**j**; 639 nm), and all three lasers (**k**) in striatal sections of 3-NP–treated rat at 28 days post-lesion. Note that intensely autofluorescent granules are clearly detected within cellular profiles with the yellow-green and blue lasers, while rarely being detected with the violet or red lasers. **l** Histogram of intensity profiles along the indicated area (*red arrow* in **k**) showing that autofluorescence profiles from the blue (*green dotted line*) and yellow-green (*red solid line*) lasers exhibit an overlapping pattern and are highly intense, while autofluorescence is rarely detectable using the red laser (*dark gray broken line*). *Scale bars* 50 μm for **a**–**c**, 100 μm for **d**–**g**, 10 μm for **h**–**k**

as tiny granules or punctate particles localized within cellular profiles, especially within cytoplasm but not in the DAPI-labeled nuclei (Fig. 1h, i). Moreover, both the intensity and the amount of the autofluorescence differed across cells, ranging from some cells being completely filled with intensely autofluorescent granules, to others containing only a few detectable autofluorescent granules.

To clarify the cellular identity of the autofluorescence-laden cells seen in the lesioned striatum, we applied fluorescence immunohistochemistry using two glia-specific markers: GFAP for astrocytes and Iba1 for microglia. Because very low autofluorescence was detected under the long-wavelength laser (over 650 nm after excitation at 633 nm), as shown in Fig. 1j, l, we used Alexa Fluor 647-labeled secondary antibody to minimize confounding autofluorescence signals in discerning immunolabeled signals. GFAP-immunolabeled sections revealed that round cells containing autofluorescent granules were localized within the striatal lesion abutting the astroglial scar tissue and that these autofluorescent cells were devoid of GFAP immunoreactivity (Fig. 2a, c). By contrast, immunolabeling with Iba1, a marker for resting microglia and activated microglia/macrophages (Ito et al. 1998), revealed that these autofluorescent cells were indeed activated microglia/macrophages (Fig. 2b, d). Under higher magnification (Fig. 2e–h), we could identify two main morphologically distinct types of microglia/macrophages in the lesion: brain macrophages having round, amoeboid cytoplasm with rare projecting processes, and activated microglia with ovoid cell bodies and short, thick processes. Intracellular localization

of autofluorescent granules and Iba1 immunoreactivity in activated microglia/macrophages revealed a complementary pattern: brain macrophages filled with autofluorescent granules revealed very weak Iba1 immunoreactivity, while activated microglia revealed intense Iba1 immunoreactivity but scant autofluorescent granules (Fig. 2h). This finding was further supported by quantitative analysis of the mean intensity profiles of the Iba1 signal and the autofluorescence signal within activated microglia/macrophages. As shown in Fig. 2i–k, the scatterplots of the Iba1 and autofluorescence signals were negatively correlated within these cells [correlation coefficient $(r) = -0.77$, $R^2 = 0.5933$, $P < 0.001$]. In other words, the Iba1 signal was relatively weak in intensely fluorescent cytoplasm filled with granules, but was strong in cytoplasm mostly devoid of such granules.

To define further the intracellular localization of autofluorescent granules within activated microglia/macrophages, the serial set of striatal sections was immunolabeled with ED1/CD68, a marker for the lysosomal membranes of macrophages (Damoiseaux et al. 1994), or with LAMP1, a late endosomal/lysosomal marker. Autofluorescent granules and lysosomal markers were co-localized within brain macrophages, but they generally appeared to be localized in a complementary pattern (Fig. 3a–h). Autofluorescent granules occupied large area of the soma of amoeboid brain macrophages, where immunoreactivity for ED1/CD68 and LAMP1 was very weak. On the other hand, the two lysosomal makers were intense in areas where autofluorescent granules were not prominent.

To examine further whether autofluorescent brain macrophages increase within striatal lesions over time after 3-NP injection, the number of ED1/CD68-positive cells and the number of autofluorescence-emitting cells among ED1/CD68-positive cells was quantified. The total number of ED1/CD68-positive cells, whether autofluorescent or not, increased progressively from day 3 through day 28 post-lesion (Fig. 3i, j). Autofluorescence-emitting brain macrophages accounted for $32.0 \pm 5.4\%$ of all macrophages at day 3, but $92.0 \pm 2.1\%$ at day 28.

Light microscopic imaging alone was not sufficient to clarify the identity of the autofluorescent granules. To characterize these signals further, we combined conventional EM with pre-embedding immuno-electron microscopy. Conventional EM demonstrated that amoeboid macrophages were abundant in the lesion core of the injured striatum at day 28, and that their cytoplasm was filled with the classical features of polymorphous lipofuscin-like granules: lipid-rich lipofuscin droplets, multi-lamellated inclusion bodies, and electron-dense fibrillary structures (Miyagishi et al. 1967; Boellaard et al. 2004; Markelic et al. 2013) (Fig. 4a, b). In addition, Iba1-positive brain macrophages revealed abundant lipofuscin-like granules
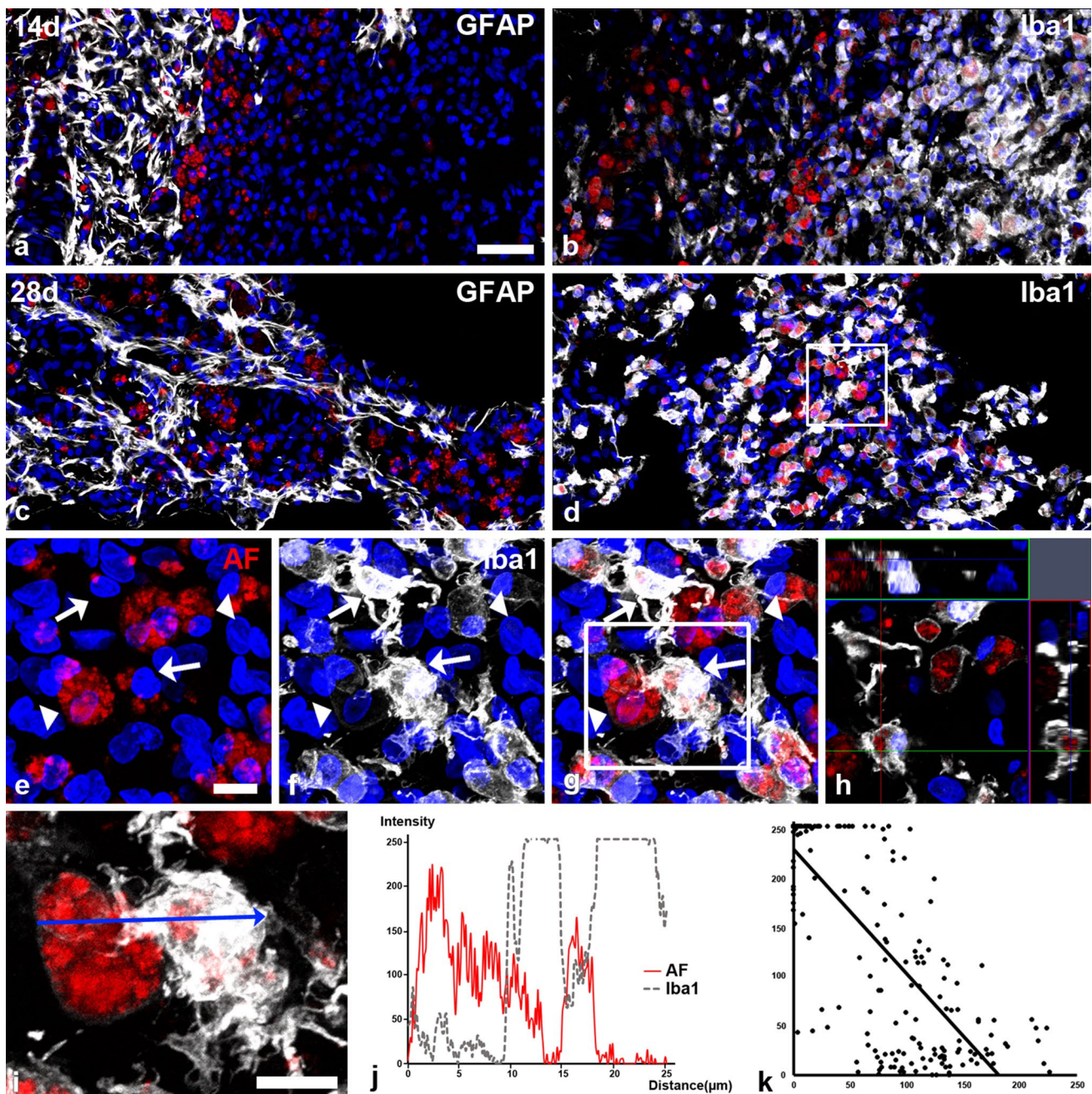
Fig. 2 Localization of autofluorescence relative to cell types in the 3-NP-injected striatum. Immunoreactivity for GFAP or Iba1 showing that almost all autofluorescent signals co-localize with Iba1-positive microglia (**b**, **d**), and not with GFAP-positive astrocytes (**a**, **c**) at 14 days (**a**, **b**), and 28 days (**c**, **d**) post-lesion. Higher-magnification views of the lesion core (*boxed area* in **d**) showing that the autofluorescent granules (AF) are localized within the cytoplasm of activated microglia/macrophages, with two complementary localization patterns seen for autofluorescent granules and Iba1 immunoreactivity. Round, amoeboid macrophages filled with autofluorescent granules show very weak Iba1 immunoreactivity (*arrowheads*), while activated microglia with intense Iba1 immunoreactivity show scanty autofluorescent granules (*arrows*). Complimentary patterns of autofluorescence and Iba1 immunoreactivity are also shown in orthogonal view (**h**). **i** Higher-magnification view of the *boxed area* in **g**. **j** Histograms of intensity profiles of Iba1-positive signal and autofluorescence along the indicated area (*blue arrow*) in **i**. Note that Iba1-positive signal and autofluorescence show largely complementary patterns within activated microglia/macrophages. **k** Scatterplot of Iba1 versus autofluorescence along the area indicated in **i**. The *x*- and *y*-axis represent the intensity of autofluorescence and of Iba1-positive signal, respectively. *Scale bars* 50 μm for **a–d**, 10 μm for **e–i**
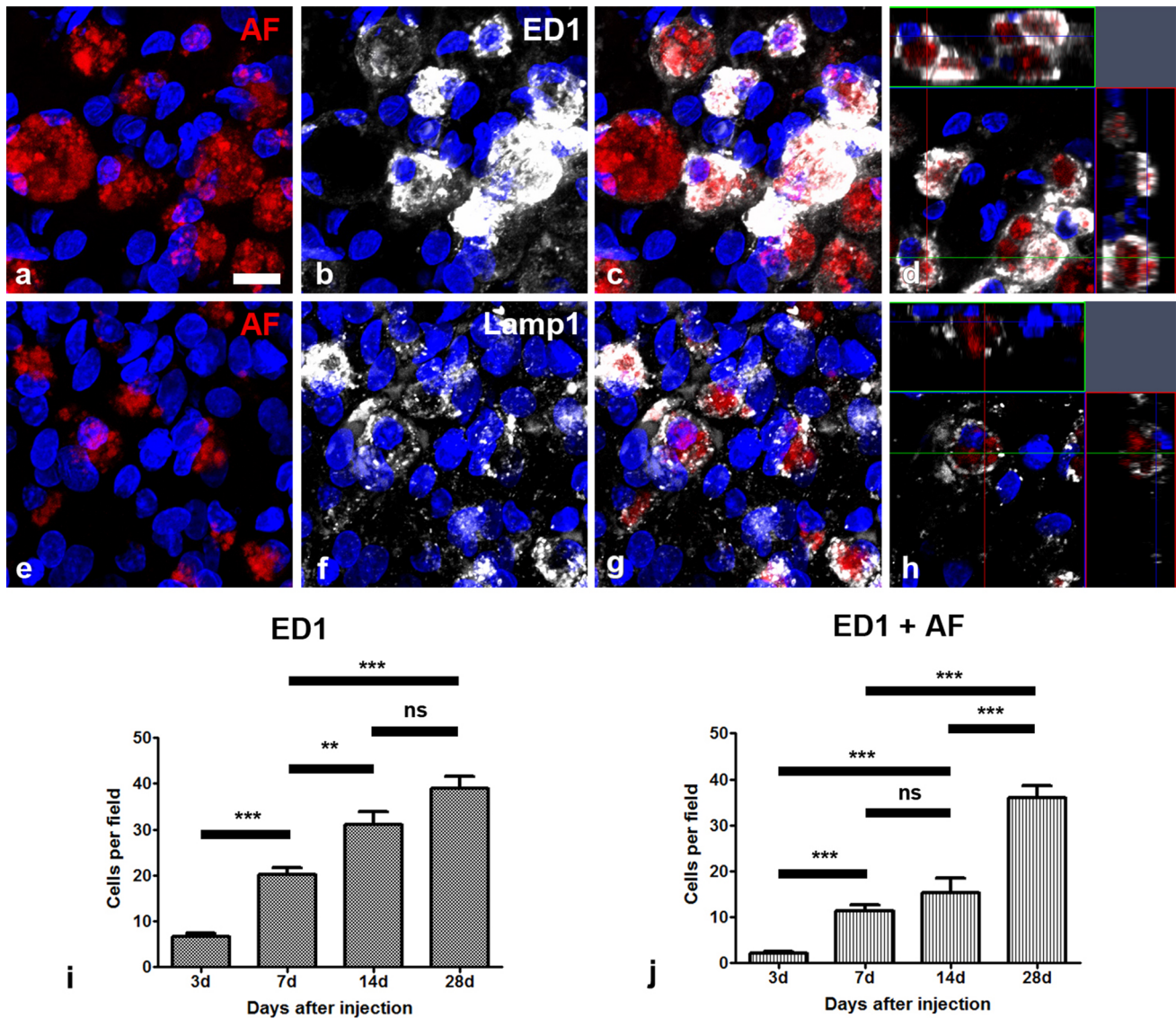
Fig. 3 Localization of autofluorescence relative to lysosomes in the 3-NP–injected striatum. **a–h** Immunoreactivities of lysosomal markers LAMP1 and ED1/CD68 at 28 days post-lesion showing that autofluorescent granules (AF) and two lysosomal markers co-localize within brain macrophages, where they are generally localized in a complimentary pattern. Quantitative analysis of the number of ED1/ CD68-positive cells (**i**) and autofluorescence-emitting, ED1/CD68-positive cells (**j**) in the striatal lesion core of 3-NP–treated rats at 3, 7, 14, and 28 days post-treatment. The data are expressed as the mean ± SEM. *$P < 0.05$; **$P < 0.01$; ***$P < 0.001$; *ns* not significant. *Scale bars* 10 μm for **a–h**

in their cytoplasm. Electron-dense grains visualized by DAB staining were localized in the periphery of the cytoplasm of these cells where lipofuscin-like inclusions were absent (Fig. 4c, d). Since Sudan Black B is used to identify lipofuscin pigments (Robles 1978; Papka et al. 1981), we performed Sudan Black B staining to prove the existence of lipofuscin in amoeboid autofluorescent macrophages, using the method of serial sections. The distribution pattern, shape, and size of round cells filled with Sudan Black B-positive granules were remarkably similar

to those of autofluorescent macrophages in the lesion core of the injured striatum (Fig. 4e–h).

Conventional and pre-embedding immuno-EM methods only indicate an indirect link between ultrastructurally characterized lipofuscin-like granules and autofluorescent signals observed with confocal microscopy. Therefore, we incorporated a correlative light and electron microscopic method to localize precisely these light microscopic signals to specific organelles and subcellular structures in brain macrophages at the level of electron microscopy. Semithin
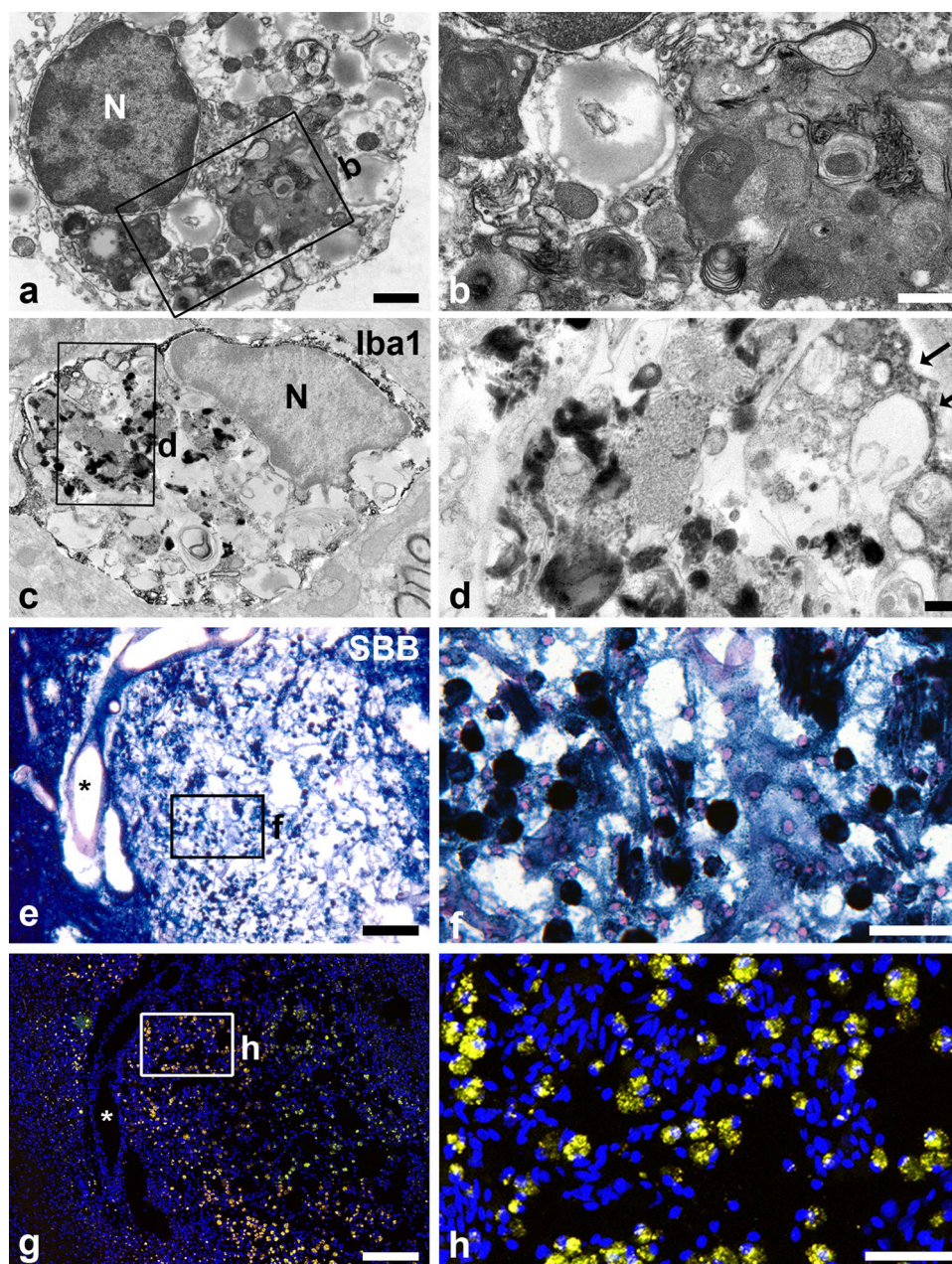
Fig. 4 Characterization of autofluorescent macrophages in the lesioned striatum at 28 days after 3-NP injection using electron microscopy and Sudan Black B staining. **a**, **b** Conventional electron microscopic images of phagocytic macrophages. Note that brain macrophages contain polymorphous lipofuscin-like granules, including lipid-rich lipofuscin droplets, multi-lamellated inclusion bodies, and electron-dense fibrillary structures. **c**, **d** Pre-embedding electron microscopic images immunostained with the microglial marker Iba1. Numerous lipofuscin-like granules are present in the cytoplasm of brain macrophages that are devoid of Iba1 immunoreactivity. Note that Iba1 immunostaining (*arrows*) only marks the plasma membranes of macrophages. **e**, **f** Sudan Black B (SBB) staining of the injured striatum. Granules stained with Sudan Black B completely fill the cytoplasm of cells resembling brain macrophages. **g**, **h** Consecutive tissue sections are viewed under yellow-green and blue laser, showing brain macrophages filled with autofluorescent granules. Note that Sudan Black B-stained cells match well with autofluorescent macrophages based on their shape and localization in the lesion core. Higher-magnification views of the boxed areas in **a**, **c**, **e**, and **g**, respectively. *Scale bars* 1 μm for **a** and **c**, 0.5 μm for **b**, 0.2 μm for **d**, 200 μm for **e** and **g**, and 50 μm for **f** and **h**; *features used to match adjacent serial sections

sections labeled with Iba1 were first observed by confocal microscopy, and the same sections were subsequently processed further for examination with electron microscopy. In

the striatum of saline-treated control rats, autofluorescence was absent in resting microglia, which had characteristic oval nuclei with dense, clumped heterochromatin and scant

Fig. 5 Absence of autofluorescent signals in resting microglia in saline-treated striatum. Confocal microscopic image of semithin section immunolabeled with Iba1 (**a**) and corresponding transmission electron microscopic image (**c**) of the same field within the striatum. **b** Overlay image of confocal microscopic data onto the corresponding electron microscopic image. Note that Iba1-labeled microglia show characteristic oval and heterochromatic nuclei and scant cytoplasm. M, resting microglia. *Scale bars* 5 μm for **a–c**
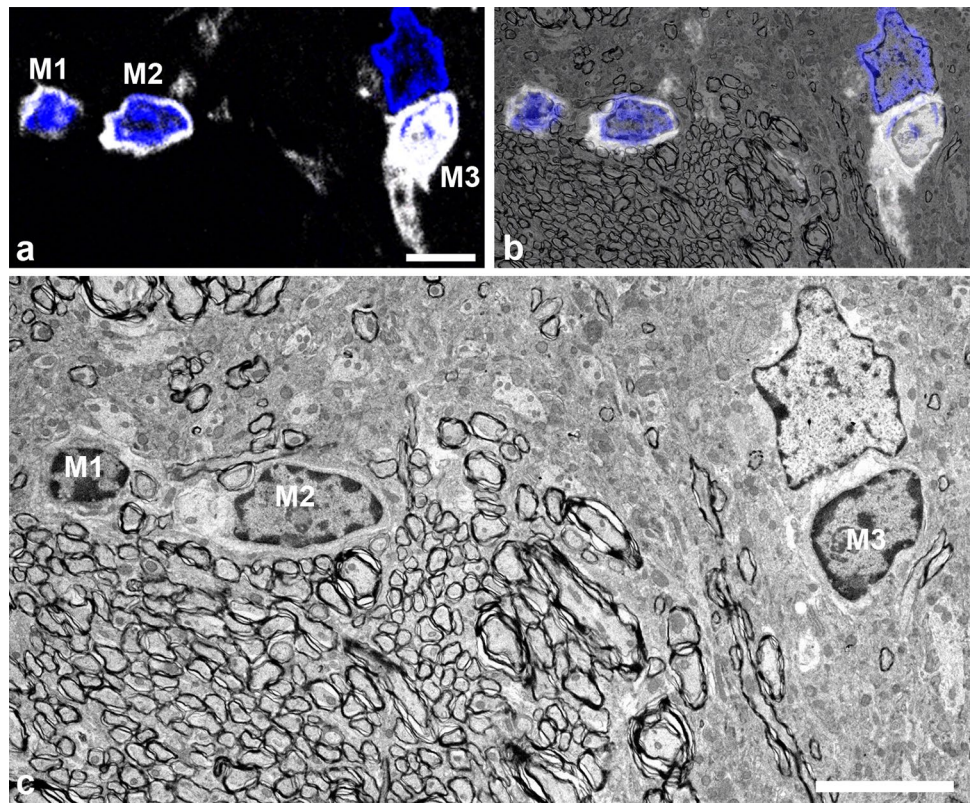
cytoplasm (Fig. 5). However, the confocal microscopy and TEM data from lesioned striatum at day 14 post-lesion revealed that these autofluorescence-emitting brain macrophages contained numerous deposits of lipofuscin-like inclusions, but had few conspicuous cytoplasmic organelles (Fig. 6a–c). The lipofuscin-like granules were identified by their polymorphous electron-dense contents as shown at higher magnification (Fig. 6d–f), which showed granular, fibrillar, or lamellated patterns closely resembling the pattern shown in conventional or pre-embedding immuno-electron findings (Fig. 4a–d). In contrast, the cytoplasm corresponding to Iba1-positive signal in activated microglia/macrophages contained cytoplasmic organelles, including mitochondria and Golgi complex, but no lipofuscin-like inclusions (Fig. 6d, e).

Discussion

In this study, we demonstrated accumulation of autofluorescent cells within sites of intense neuronal damage from 14 days post–3-NP injection onward. Confocal microscopic findings from sections immunolabeled with Iba1 revealed these autofluorescent cells to be activated microglia/macrophages. Autofluorescent granules were increased in number and intensity in amoeboid-like brain macrophages compared with those of stellate microglia with

evident processes. Interestingly, autofluorescent granules and the calcium-binding protein Iba1 had non-overlapping, even complementary, distributions within activated microglia/macrophages. Two lysosomal markers, ED1/CD68 and LAMP1, also exhibited labeling patterns complementary with autofluorescent granules within the cytoplasm of these cells. Thus, these data indicate that autofluorescent granules usually accumulated within the lysosome-free cytoplasm of activated microglia/macrophages. In addition, our data show a regional correlation of autofluorescent macrophages with cells stained with Sudan Black B, a well-known method of visualizing lipofuscin in tissues or cells (Robles 1978; Papka et al. 1981). By means of a correlative approach using light and electron microscopy (an excellent tool for the detailed ultrastructural study of specific targets), we confirmed that these light-microscopic, autofluorescent granules corresponded to clusters of lipofuscin-like granules with various morphologies.

Lipofuscin is regarded as undigested intracellular waste originating from a variety of intracellular structures, and accumulates in the lysosomes of post mitotic cells (Miyagishi et al. 1967; Brunk and Terman 2002; Boellaard et al. 2004). It is well known that lipofuscin contains several fluorophores that can be visualized by fluorescence microscopy (Terman and Brunk 1998; Gray and Woulfe 2005). Several reports mention autofluorescent microglial cells containing lipofuscin granules. Notably, retinal
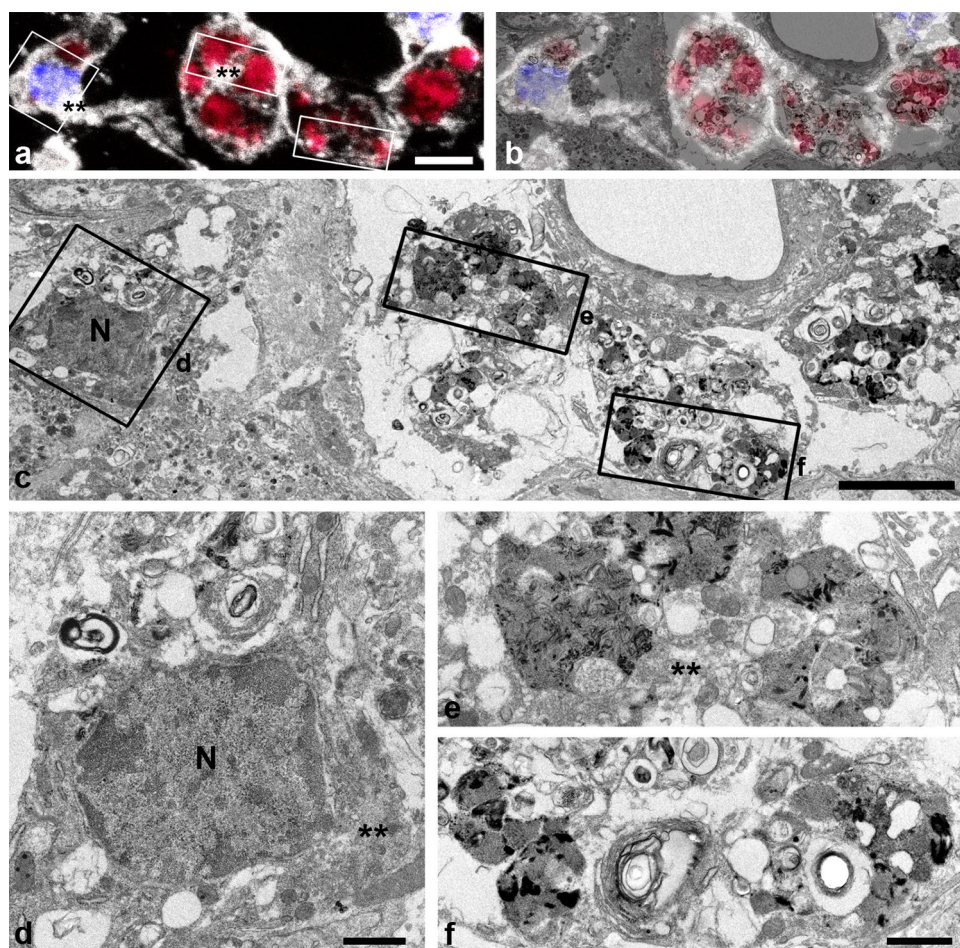
Fig. 6 Ultrastructural localization of autofluorescent granules in the 3-NP–injected striatum using correlative light and electron microscopy. Within the striatal lesion 14 days after 3-NP injection, we show a confocal microscopic image of a semithin section immunolabeled with Iba1 (**a**) and the corresponding transmission electron microscopic image (**c**) of the same field. Immunolabeled Iba1 appears white and autofluorescent signals appear *red*. **b** Overlay image of confocal microscopic data onto the corresponding electron microscopic image. **d–f** Higher-magnification views of the boxed areas in **a** and **c**. Note that autofluorescent brain macrophages contain numerous deposits of lipofuscin-like inclusions, but have few conspicuous cytoplasmic organelles. Lipofuscin-like inclusions appear as polymorphous, electron-dense material with granular, fibrillar, or lamellated morphology. Also note that the cytoplasm corresponding to Iba1-positive signal in activated microglia/macrophages contains cytoplasmic organelles, including mitochondria and Golgi complex, but no lipofuscin-like inclusions (*asterisks* in **a**, **d**, and **e**). Cell nuclei appear blue after DAPI staining. *N* nucleus. *Scale bars* 5 μm for **a–c**, 1 μm for **d–f**

perivascular microglia, subretinal microglia, and retinal macrophages have all shown lipofuscin-like autofluorescence (Xu et al. 2008; Mendes-Jorge et al. 2009; Lei et al. 2012), and microglia in the main olfactory bulb have shown autofluorescence due to the presence of lipofuscin granules. In addition, Molcanyi et al. (2013) reported that activated microglia/macrophages could be a significant source of nonspecific fluorescence after traumatic brain injury. Thus, our data reinforce the idea that activated microglia/macrophages can exhibit autofluorescence and we provide new evidence identifying their autofluorescent granules as accumulated lipofuscin-like granules.

An interesting finding of the present study is that brain macrophages containing only a few intact lysosomes or cytoplasmic organelles were overloaded with phagocytosed waste materials, i.e., lipofuscin-like granules. Thus, it is likely that those brain macrophages having relatively more lipofuscin-like granules were less capable of digesting further phagocytic materials, thereby exaggerating the accumulation of intensely autofluorescent granules within them. This suggestion was additionally supported by the observation of a negative correlation between Iba1 signals and autofluorescence within activated microglia/macrophages in 3-NP-induced striatal lesions (see Fig. 2k). Iba1 is involved in the Rho family of small GTPases/Rac/calcium signaling pathway and is required for cell mobility and phagocytosis (Ohsawa et al. 2000; Sasaki et al. 2001; Kanazawa et al. 2002). Therefore, observation of

microglia/macrophages with increased autofluorescence and low expression of Iba1 might imply a reduction in their phagocytic activity. In addition, our data revealed that autofluorescent brain macrophages tended to increase in number and intensity within striatal lesions over time after 3-NP injection. This observation was confirmed by a quantitative study showing a time-dependent accumulation of autofluorescence-emitting brain macrophages after 3-NP injection. Considered together, our data indicate that the occurrence of autofluorescent brain macrophages correlates with the progression of neurodegeneration after brain insults, suggesting that the intensity of autofluorescence in these cells can reflect their activated functional status induced by brain insults, which involves phagocytic activity.

A number of techniques have been suggested to reduce or eliminate autofluorescence due to lipofuscin, such as quenching dyes, photo bleaching, and treatment of brain sections with sodium borohydride/cupric sulfate/ammonium-acetate buffer (Schnell et al. 1999; Oliveira et al. 2010; Spitzer et al. 2011; Davis et al. 2014; Sun and Chakrabartty 2016). Nevertheless, it is difficult to choose a suitable technique because the effectiveness of such techniques depends on the type of cells or tissue, fixation, processing, and wavelength of excitation light. Instead, we recommend greater circumspection in selecting appropriate fluorophore-labeled secondary antibodies when performing double- or triple-labeling immunohistochemistry with injured brain tissues. Our data revealed that the fluorescence of lipofuscin-like granules within activated microglia/macrophages has an excitation wavelength ranging from 488 to 555 nm and an emission wavelength ranging from 523 to 573 nm, which overlap with the excitation and emission spectra of commonly used fluorophores such as fluorescein isothiocyanate (FITC), cyanine 2 (Cy2), cyanine 3 (Cy3), and tetramethyl rhodamine isothiocyanate (TRITC). Thus, the autofluorescence of lipofuscin-like granules could interfere with the detection of these exogenous fluorophores in the same detection region. By contrast, the autofluorescence arising from lipofuscin-like granules decreased dramatically in the long wavelength region (639 nm), so that it did not overlap with the excitation or emission spectra of Alexa Fluor 647-conjugated antibodies in the lesioned striatum. Thus, we suggest that Alexa Fluor 647-conjugated antibodies or other fluorophore-labeled antibodies with similar optical profiles, such as Cy5, might be the proper choice when choosing fluorophores for the immunofluorescence of target proteins within activated microglia/macrophages after brain insults.

In summary, the present study demonstrates that autofluorescence tends to increase within the striatal lesion over time after 3-NP injection, which is attributable to an accumulation of lipofuscin-like inclusions within activated microglia/macrophages. Thus, our data indicate that special care should be taken when verifying unknown fluorescent signals likely to be especially correlated with microglia/macrophages activated by brain insults.

Compliance with ethical standards

Conflict of interest The authors declare that they have no conflict of interest.

References

Amenta D, Ferrante F, Franch F, Amenta F (1988) Effects of long-term Hydergine administration on lipofuscin accumulation in senescent rat brain. Gerontology 34(5–6):250–256

Aubin JE (1979) Autofluorescence of viable cultured mammalian cells. J Histochem Cytochem Off J Histochem Soc 27(1):36–43

Banerjee B, Miedema BE, Chandrasekhar HR (1999) Role of basement membrane collagen and elastin in the autofluorescence spectra of the colon. J Investig Med Off Publ Am Feder Clin Res 47(6):326–332

Boellaard JW, Schlote W, Hofer W (2004) Species-specific ultrastructure of neuronal lipofuscin in hippocampus and neocortex of subhuman mammals and humans. Ultrastruct Pathol 28(5–6):341–351. doi:10.1080/019131290882330

Brizzee KR, Ordy JM, Kaack B (1974) Early appearance and regional differences in intraneuronal and extraneuronal lipofuscin accumulation with age in the brain of a nonhuman primate (*Macaca mulatta*). J Gerontol 29(4):366–381

Brooke SM, Trafton JA, Sapolsky RM (1996) Autofluorescence as a confound in the determination of calcium levels in hippocampal slices using fura-2AM dye. Brain Res 706(2):283–288

Brunk UT, Terman A (2002) Lipofuscin: mechanisms of age-related accumulation and influence on cell function. Free Radical Biol Med 33(5):611–619

Chung YG, Schwartz JA, Gardner CM, Sawaya RE, Jacques SL (1997) Diagnostic potential of laser-induced autofluorescence emission in brain tissue. J Korean Med Sci 12(2):135–142. doi:10.3346/jkms.1997.12.2.135

Crespi F, Croce AC, Fiorani S, Masala B, Heidbreder C, Bottiroli G (2004) In vivo autofluorescence spectrofluorometry of central serotonin. J Neurosci Methods 140(1–2):67–73. doi:10.1016/j.jneumeth.2004.06.019

Croce AC, Spano A, Locatelli D, Barni S, Sciola L, Bottiroli G (1999) Dependence of fibroblast autofluorescence properties on normal and transformed conditions. Role of the metabolic activity. Photochem Photobiol 69(3):364–374

Damoiseaux JG, Dopp EA, Calame W, Chao D, MacPherson GG, Dijkstra CD (1994) Rat macrophage lysosomal membrane antigen recognized by monoclonal antibody ED1. Immunology 83(1):140–147

Davis AS, Richter A, Becker S, Moyer JE, Sandouk A, Skinner J, Taubenberger JK (2014) Characterizing and diminishing autofluorescence in formalin-fixed paraffin-embedded human respiratory tissue. J Histochem Cytochem Off J Histochem Soc 62(6):405–423. doi:10.1369/0022155414531549

Gray DA, Woulfe J (2005) Lipofuscin and aging: a matter of toxic waste. Science of aging knowledge environment: SAGE KE 2005 (5):re1. doi:10.1126/sageke.2005.5.re1

Hamilton BF, Gould DH (1987) Nature and distribution of brain lesions in rats intoxicated with 3-nitropropionic acid: a type of hypoxic (energy deficient) brain damage. Acta Neuropathol 72(3):286–297

Ito D, Imai Y, Ohsawa K, Nakajima K, Fukuuchi Y, Kohsaka S (1998) Microglia-specific localisation of a novel calcium binding protein, Iba1. Brain Res Mol Brain Res 57(1):1–9

Jung T, Bader N, Grune T (2007) Lipofuscin: formation, distribution, and metabolic consequences. Ann NY Acad Sci 1119:97–111. doi:10.1196/annals.1404.008

Kanazawa H, Ohsawa K, Sasaki Y, Kohsaka S, Imai Y (2002) Macrophage/microglia-specific protein Iba1 enhances membrane ruffling and Rac activation via phospholipase C-gamma -dependent pathway. J Biol Chem 277(22):20026–20032. doi:10.1074/jbc.M109218200

Lei L, Tzekov R, Tang S, Kaushal S (2012) Accumulation and autofluorescence of phagocytized rod outer segment material in macrophages and microglial cells. Molecular vision 18:103–113

Liu S, Connor J, Peterson S, Shuttleworth CW, Liu KJ (2002) Direct visualization of trapped erythrocytes in rat brain after focal ischemia and reperfusion. J Cereb Blood Flow Metab Off J Int Soc Cereb Blood Flow Metab 22(10):1222–1230. doi:10.1097/00004647-200210000-00010

Markelic M, Velickovic K, Golic I, Klepal W, Otasevic V, Stancic A, Jankovic A, Vucetic M, Buzadzic B, Korac B, Korac A (2013) The origin of lipofuscin in brown adipocytes of hyperinsulinaemic rats: the role of lipid peroxidation and iron. Histol Histopathol 28(4):493–503. doi:10.14670/hh-28.493

Mendes-Jorge L, Ramos D, Luppo M, Llombart C, Alexandre-Pires G, Nacher V, Melgarejo V, Correia M, Navarro M, Carretero A, Tafuro S, Rodriguez-Baeza A, Esperanca-Pina JA, Bosch F, Ruberte J (2009) Scavenger function of resident autofluorescent perivascular macrophages and their contribution to the maintenance of the blood–retinal barrier. Invest Ophthalmol Vis Sci 50(12):5997–6005. doi:10.1167/iovs.09-3515

Miyagishi T, Takahata N, Iizuka R (1967) Electron microscopic studies on the lipo-pigments in the cerebral cortex nerve cells of senile and vitamin E deficient rats. Acta Neuropathol 9(1):7–17

Molcanyi M, Bosche B, Kraitsy K, Patz S, Zivcak J, Riess P, El Majdoub F, Hescheler J, Goldbrunner R, Schafer U (2013) Pitfalls and fallacies interfering with correct identification of embryonic stem cells implanted into the brain after experimental traumatic injury. J Neurosci Methods 215(1):60–70. doi:10.1016/j.jneumeth.2013.02.012

Monici M (2005) Cell and tissue autofluorescence research and diagnostic applications. Biotechnol Ann Rev 11:227–256. doi:10.1016/s1387-2656(05)11007-2

Ohsawa K, Imai Y, Kanazawa H, Sasaki Y, Kohsaka S (2000) Involvement of Iba1 in membrane ruffling and phagocytosis of macrophages/microglia. J Cell Sci 113(Pt 17):3073–3084

Oliveira VC, Carrara RC, Simoes DL, Saggioro FP, Carlotti CG Jr, Covas DT, Neder L (2010) Sudan Black B treatment reduces autofluorescence and improves resolution of in situ hybridization specific fluorescent signals of brain sections. Histol Histopathol 25(8):1017–1024

Ottis P, Koppe K, Onisko B, Dynin I, Arzberger T, Kretzschmar H, Requena JR, Silva CJ, Huston JP, Korth C (2012) Human and rat brain lipofuscin proteome. Proteomics 12(15–16):2445–2454. doi:10.1002/pmic.201100668

Papka R, Peretz B, Tudor J, Becker J (1981) Age-dependent anatomical changes in an identified neuron in the CNS of *Aplysia californica*. J Neurobiol 12(5):455–468. doi:10.1002/neu.480120505

Paxinos G, Watson C (1998) A stereotaxic atlas of the rat brain. Academic, New York

Robles LJ (1978) Accumulation and identification of lipofuscin-like pigment in the neurons of *Bulla gouldiana* (Gastropoda: Opisthobranchia). Mech Ageing Dev 7(1):53–64

Sasaki Y, Ohsawa K, Kanazawa H, Kohsaka S, Imai Y (2001) Iba1 is an actin-cross-linking protein in macrophages/microglia. Biochem Biophys Res Commun 286(2):292–297. doi:10.1006/bbrc.2001.5388

Schnell SA, Staines WA, Wessendorf MW (1999) Reduction of lipofuscin-like autofluorescence in fluorescently labeled tissue. J Histochem Cytochem Off J Histochem Soc 47(6):719–730

Spanswick SC, Bray D, Zelinski EL, Sutherland RJ (2009) A novel method for reliable nuclear antibody detection in tissue with high levels of pathology-induced autofluorescence. J Neurosci Methods 185(1):45–49. doi:10.1016/j.jneumeth.2009.09.007

Spitzer N, Sammons GS, Price EM (2011) Autofluorescent cells in rat brain can be convincing impostors in green fluorescent reporter studies. J Neurosci Methods 197(1):48–55. doi:10.1016/j.jneumeth.2011.01.029

Sun Y, Chakrabartty A (2016) Cost-effective elimination of lipofuscin fluorescence from formalin-fixed brain tissue by white phosphor light emitting diode array. Biochem Cell Biol Biochimie et biologie cellulaire 94(6):545–550. doi:10.1139/bcb-2016-0125

Terman A, Brunk UT (1998) Lipofuscin: mechanisms of formation and increase with age. APMIS: Acta Pathologica, Microbiologica, et Immunologica Scandinavica 106(2):265–276

Viegas MS, Martins TC, Seco F, do Carmo A (2007) An improved and cost-effective methodology for the reduction of autofluorescence in direct immunofluorescence studies on formalin-fixed paraffin-embedded tissues. Eur J Histochem EJH 51(1):59–66

Xu H, Chen M, Manivannan A, Lois N, Forrester JV (2008) Age-dependent accumulation of lipofuscin in perivascular and sub-retinal microglia in experimental mice. Aging Cell 7(1):58–68. doi:10.1111/j.1474-9726.2007.00351.x